Generation of Rydberg states of hydrogen atoms with intense laser pulses: The roles of Coulomb force and initial lateral momentum

Bin Zhang, Wenbo Chen, and Zengxiu Zhao*

Department of Physics, College of Science, National University of Defense Technology, Changsha, Hunan 410073, China

(Received 12 June 2014; published 8 August 2014)

We investigate the generation of Rydberg states of hydrogen atoms with intense laser pulses by solving the time-dependent Schrödinger equation and by means of classical-trajectory Monte Carlo simulations. Both linearly polarized multicycle pulses and pairs of optical half-cycle pulses are used. Comparisons between these methods show that both the Coulomb force and initial lateral momentum, which have effects on the n distribution and l distribution of the population of excited states, are important in the generation of Rydberg states.

DOI: 10.1103/PhysRevA.90.023409 PACS number(s): 32.80.Rm, 42.50.Hz, 42.65.Ky

I. INTRODUCTION

Tunnel ionization is a fundamental atomic and molecular process in strong laser fields [1]. The tunneled electron is accelerated in the fields and may return to the vicinity of the ion, resulting in many highly nonlinear strong-field phenomena, such as high-harmonic generation, above-threshold ionization, and nonsequential double ionization [2]. A recent experiment showed that in the strong-field tunnel ionization of helium atoms, a substantial fraction of Rydberg atoms was produced and measured in the intense laser pulse, which was explained with the strong-field tunneling-plus-rescattering model and named frustrated tunneling ionization (FTI) [3]. FTI is the completion of the tunneling-rescattering scenario.

The neglect of Coulomb force after ionization in the classical three-step model [4] and quantum Lewenstein model [5] works surprisingly well to explain the process of high-harmonic generation. For the generation of Rydberg states, a semiclassical model [6] that neglected Coulomb force during the laser pulse was used to explain the experimentally measured dependence of the excited-state population on the ellipticity of the laser pulses [3]. However, more recently, the role of the Coulomb force has drawn considerable attention, and the inclusion of the Coulomb force has proven to be essential in many studies [7–12]. While some progress has been made in analyzing the generation of Rydberg states in both elliptically [6] and linearly polarized light [13], the underlying physics, especially the role of Coulomb force, still remain to be explained. We will also investigate the role of the initial lateral momentum distribution with respect to the tunneling process [14].

Previous investigations focused on the generation of Rydberg atoms with multicycle laser pulses [6,13,15,16]. In this paper, we first present some results utilizing the multicycle laser pulses. To filter out the complexity and gain better insight into the underlying mechanism, we have also utilized a pair of optical half-cycle pulses (HCP). The HCP fields in the frequency of the terahertz (THz) regime have been widely used in investigating and controlling the Rydberg states in the past [17–24]. If the pulse duration of a HCP is very short compared to the orbital time of a Rydberg electron [25], the impact of this HCP is generally described as a momentum kick [17]. No studies have been done using the HCPs in the frequency of the optical regime. Such optical HCPs have several advantages against THz HCPs: (1) Due to the weak intensity, the THz HCP can only be used to generate a THz Rydberg wave packet (a superposition of the initial state and its neighboring states) [19] from an initial optically excited atom. (2) The pulse duration of THz HCP is of (or near) the same order as the orbital time of a highly excited Rydberg electron [19], thus mixing the interaction with more complex wave-packet dynamics and making the "kick" description less valid. (3) For the ground and low-lying excited states, the interaction with THz HCP is difficult to treat in an ab-initio way since the electron moves at an attosecond time scale [2]. The theoretical investigation of Rydberg state generation with optical HCPs is thus meaningful and may provide insights into the underlying physics.

The organization of this paper is as follows: In Sec. II we briefly describe the methods of solving the three-dimensional (3D) time-dependent Schrödinger equation (TDSE) and classical-trajectory Monte Carlo (MC) simulation. Section III gives the calculation details. In Sec. IV, we present our results and discussion in detail. We conclude in Sec. V.

II. THEORY

A. Time-dependent Schrödinger equation

The TDSE for atomic hydrogen in the presence of external laser fields [$\mathbf{F}(t)$] can be written as [atomic units (a.u.) are used unless otherwise stated]

$$i\frac{\partial\Psi(\mathbf{r},t)}{\partial t} = [H_0 + V(\mathbf{r},t)]\Psi(\mathbf{r},t), \tag{1}$$

where the field-free Hamiltonian $H_0 = -\nabla^2/2 - 1/r$ and laser-atom interaction $V(\mathbf{r},t) = \mathbf{F}(t)\cdot\mathbf{r}$. The orbital $\Psi(\mathbf{r},t)$ is expanded in the spherical harmonics,

$$\Psi(\mathbf{r},t) = \sum_{l=0}^{l_{\max}}\sum_{m=-l}^{m=l}\frac{\phi_{lm}(r,t)}{r}Y_{lm}(\theta,\varphi). \tag{2}$$

For linearly polarized laser fields, the expansion includes only the $m = 0$ partial waves.

For the r coordinate, we use the discrete variable representation (DVR) basis functions. To this purpose, the variable r is first truncated from the semi-infinite $(0,\infty)$ domain into the finite domain $(0,r_{\max}]$ (with sufficiently large $r_{\max}$). The r coordinate is then discretized using the generalized

*zhao.zengxiu@gmail.com

Gauss-quadrature points r^i and weights w_i^r:

$$r_i = L\frac{1+x_i}{1-x_i+\alpha}, \quad w_i^r = r_i^{'} w_i, \tag{3}$$

where the points and weights $[\{x_i,\ w_i\},\ i = 1,\ldots,n_r]$ are associated with the standard (n_r) point Gauss-Radau quadrature $(x_{n_r} = 1)$ [26]. L and $\alpha = 2L/r_{\max}$ are the mapping parameters. This mapping function $r(x)$ allows for denser grids near the origin, leading to more accurate eigenvalues and eigenfunctions [27]. The Coulomb singularity at the origin is avoided since $r_{\min} = r(x_1) > 0$.

The radial partial wave $\phi_{lm}(r,t)$ is expanded in a product basis of functions,

$$\phi_{lm}(r,t) = \sum_i c_i^{lm}(t) g_i(r), \tag{4}$$

where the DVR functions read

$$g_i(r) = \frac{1}{\sqrt{w_i^r}} \prod_{j\neq i}^{n_r} \frac{r-r_j}{r_i-r_j}. \tag{5}$$

Note that the factor $1/\sqrt{w_i^r}$ is built in to remove the integration overlaps, which results in the orthonormal condition, $\int_{r_{\min}}^{r_{\max}} g_i(r) g_j(r) dr = \delta_{ij}$ [28].

The ground and excited states of the hydrogen atom are calculated by dialogizing the ground-state Hamiltonian. Equation (1) is propagated in time by the second-order split-operator technique [28]. An absorbing layer between r_b and $r_{\max}$ is used to smoothly bring down the wave function and to prevent the unphysical reflection from the boundary. After the time propagation, we get the final wave function $\Psi(\mathbf{r},T)$. We calculate the probability of having the electron in the nlm bound state by projecting $\Psi(\mathbf{r},T)$ onto the corresponding field-free eigenstates $\Psi_{nlm}(\mathbf{r})$,

$$p_{nlm} = |\langle \Psi_{nlm}(\mathbf{r}) | \Psi(\mathbf{r},T)\rangle|^2. \tag{6}$$

The probability of having the electron in the n quantum state is $p_n = \sum_{lm} p_{nlm}$.

B. Monte Carlo

To compare with the TDSE calculations, we employ the classical-trajectory MC method including tunneling [29–31]. Tunnel ionization dominates if the Keldysh parameter $\gamma = \sqrt{2I_p}\omega/F(t_0) < 1$ [32], where I_p is the ionization potential and ω is the carrier frequency of the laser field. If the polarization direction of the laser electric fields is along the z axis, the trajectories start at time t_0 at the tunnel exit with the coordinates

$$z(t_0) = \frac{I_p + \sqrt{I_p^2 - 4F(t_0)Z_c}}{2F(t_0)}, \quad x(t_0) = y(t_0) = 0. \tag{7}$$

This expression requires $F(t_0) < I_p^2/4Z_c$, and the over-the-barrier ionization (OTBI) is avoided. In agreement with the tunneling model the initial momentum in the z direction is zero, i.e., $p_z = 0$. The probability $w_\perp$ of tunneling with a certain lateral momentum $p_\perp(t_0) = \sqrt{p_x^2(t_0) + p_y^2(t_0)}$ is given by [14]

$$w_\perp \propto |p_\perp| \exp\left(-p_\perp^2 \frac{\kappa}{F(t_0)}\right), \tag{8}$$

and the ionization probability w_0 is given by the Ammosov-Delone-Krainov (ADK) theory [1],

$$w_0 \propto \left(\frac{2\kappa^3}{F(t_0)}\right)^{2Z_c/\kappa - |m| - 1} \exp\left(-\frac{2\kappa^3}{3F(t_0)}\right). \tag{9}$$

Here, m is the magnetic quantum number, which is initially $m = 0$, and $Z_c = 1$ is the core charge. $I_p = 0.5$ a.u. is the binding energy, and $\kappa = \sqrt{2I_p}$.

Using the probabilities in Eqs. (8) and (9), we randomly pick an initial lateral momentum and an initial ionization time t_0. The electron is then propagated by integrating Newton's equations, under the combined field of the laser field and Coulomb force,

$$\frac{d^2\mathbf{r}}{dt^2} = -\mathbf{F}(t) + \nabla(1/r). \tag{10}$$

After the laser pulse, we evaluate the total energy $E = p^2/2 - 1/r$, where $p = \sqrt{p_z^2 + p_\perp^2}$ is the momentum of the electron. If E is negative, the electron is bounded, and we determine an effective principal quantum number n_{eff} and an effective angular momentum number l_{eff} from

$$E = -\frac{1}{2n_{\text{eff}}^2}, \quad |\mathbf{L}|^2 = l_{\text{eff}}(l_{\text{eff}}+1), \tag{11}$$

where the classical angular momentum reads $\mathbf{L} = \mathbf{r}\times\mathbf{v} = (r_\parallel v_\perp - r_\perp v_\parallel)\mathbf{e}_\parallel \times \mathbf{e}_\perp$. To compare with the quantum results from TDSE calculations, the probabilities with n_{eff} and l_{eff} are integrated within each unit interval. If $v_\parallel = 0$, we find $l = n - 1$, corresponding to a circular Rydberg state.

III. CALCULATION

For the TDSE calculations, a high l quantum number should be used in the partial wave expansion in Eq. (2) if the hydrogen atom is subjected to intense laser fields. For the laser pulses we have used in this paper, convergency is reached at $l_{\max} = 80$. For hydrogen atoms, according to the classical Bohr-Sommerfeld model, the orbital radius scales as n^2 and $2n^2$ for $l = n - 1$ and $l = 0$ for the principal quantum number n [25]. In this paper, we investigate the Rydberg states generation of hydrogen atoms with $n \leqslant 40$, which results in a simulation box as large as $r_{\max} \approx 3000$ a.u. The size of the Gauss-Radau quadrature $n_r = 2000$. For this large simulation box, the dipole approximation is still valid for the 800-nm laser fields.

The ground and excited states of hydrogen atoms are calculated accurately by dialogizing the field-free Hamiltonian H_0, and the energy of the ground state $E_{1s} = -0.499999999998$ a.u., with a relative error of 10^{-12} compared to the exact value (0.5 a.u.). For the split-operator propagation scheme, the field-free propagator $\exp(-i\frac{1}{2}\Delta t H_0)$ only needs to be constructed once before the propagation, using the energy values and eigenstates of the unperturbed system. To improve the numerical stability of the propagation, a cutoff in the energy is applied to get rid of the spurious transitions to the irrelevant regions of the very high energy

spectrum. The external field operator $\exp[-i\Delta t V(t)]$ is diagonal in the coordinate representation when using the length gauge. The time step for the propagation takes $\Delta t = 0.01$ a.u. For efficient matrix and vector operations we use the basic linear algebra subroutines (BLAS) [33] and the linear algebra package (LAPACK) [34].

For the MC simulations, about 2×10^6 trajectories have been launched every optical cycle at each fixed laser intensity while the initial lateral momentum and ionization time are randomly varied. To investigate the effects of Coulomb force and initial lateral momentum, we have also performed MC simulations (1) ignoring the Coulomb force after the electron tunnels out of the barrier [$V_c(t) = 0, t > t_0$] and (2) ignoring the initial lateral momentum distribution at the tunnel exit [$p_\perp(t_0) = 0$]. Comparisons with and discussions about TDSE calculations are given.

The multicycle laser electric field $\mathbf{F}(t)$ is chosen to be $\mathbf{F}(t) = F_0\mathbf{e}_F \sin^2(\pi t/\tau)\sin(\omega t + \delta)$, where F_0 is the peak field amplitude, τ is the pulse duration, and δ is the carrier envelope phase (CEP). In this paper, the unit of laser intensity $I_0 = 1\times10^{14}$ W/cm^2. We use multicycle pulses with a pulse duration of $10T$, where $T = 2\pi/\omega$ is the optical period. For a HCP pulse, the electric field is $\mathbf{F}(t) = F_0\mathbf{e}_F \sin(\omega t + \delta)$, with $0 \leqslant t \leqslant \tau = T/2$. The phase δ is used to control the parity of the unipolar field.

IV. RESULTS AND DISCUSSION

Figure 1 presents the sum population of excited states of $n = 20$–40 and the n quantum number of the most populated excited states for different laser intensities from TDSE calculations. The laser-pulse duration is ten optical cycles. The sum population increases rapidly for relatively weak laser intensities and reaches a plateau at higher intensities. Ionization saturation is reached at higher laser intensities, while the population of highly excited Rydberg states does not drop (in fact, there is a slight increase at intensities of 10^{15} W/cm^2 and higher). This plateau of population may

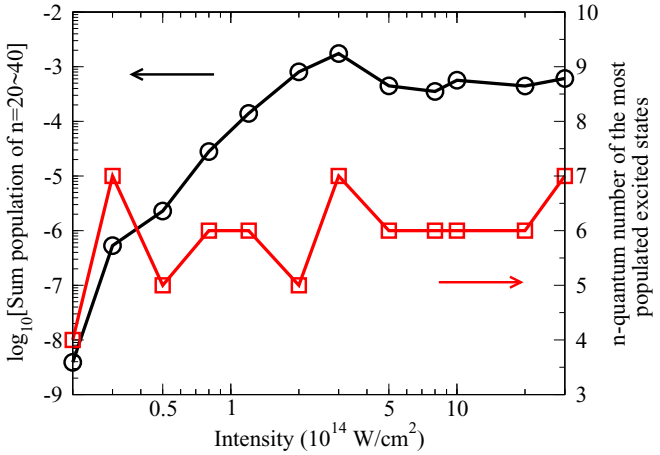

FIG. 1. (Color online) Sum population of excited states of $n = 20$–40 (circles) and the n quantum number of the most populated excited states (squares) vs the laser intensity from the TDSE calculations. The laser-pulse duration is ten optical cycles, and the carrier wavelength is 800 nm.

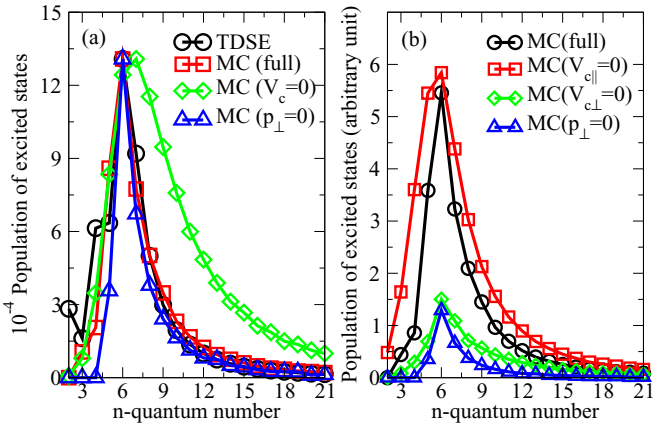

FIG. 2. (Color online) (a) n distribution of the population of excited states from a TDSE calculation (circles) and MC simulations: full (squares), $V_c = 0$ (diamonds), and $p_\perp = 0$ (triangles). The populations from MC simulations have been normalized to the maximum of the TDSE calculation at $n = 6$. (b) n distribution of the population of excited states from MC simulations: full (circles), $V_{c\parallel} = 0$ (squares), $V_{c\perp} = 0$ (diamonds), and $p_\perp = 0$ (triangles). The laser-pulse duration is ten optical cycles, and the intensity is 1.2×10^{14} W/cm^2.

be explained by the fact that highly excited Rydberg atoms can survive in very intense laser fields, as shown by the experimental investigation of helium atoms [35]. For the nonresonant 800-nm laser fields we have used, the n quantum number of the most populated excited states is insensitive to the laser intensity, yielding a principal quantum number of 6 on average.

To investigate the n distribution of the population of excited states in detail, Fig. 2(a) presents the results from TDSE calculation and MC simulations at a laser intensity of 1.2×10^{14} W/cm^2. This intensity is chosen so that tunnel ionization is satisfied while OTBI is avoided. For comparison, the MC results are normalized according to the TDSE result. For the TDSE calculation, a sharp maximum in the distribution is found around $n = 6$. The full MC simulation yields a result in good agreement with TDSE. In a previous work [13] where a laser pulse of $\omega = 0.05$ a.u. and $I = 3.5\times10^{14}$ W/cm^2 were used, the population distribution was very similar to our results: a sharp peak at $n = 6$ in the distribution. This is consistent with the conclusion of Fig. 1. If the nuclear Coulomb force is ignored in the classical propagation ($V_c = 0$), MC simulation yields a broad distribution in the high n quantum number part, in qualitative disagreement with TDSE and full MC results. This demonstrates the importance of the Coulomb force in the generation of highly excited Rydberg states. On the other hand, if the initial lateral momentum distribution is set to zero ($p_\perp = 0$), the result still seems to be in qualitative agreement with TDSE and full MC simulations.

Does the initial lateral momentum have little effect in this case? To answer this, in contrast to the normalized results in Fig. 2(a), Fig. 2(b) presents the unnormalized population results from different MC simulations. For the linearly polarized laser fields, the Coulomb force can be divided into two parts: the forces parallel ($V_{c\parallel}$) and perpendicular ($V_{c\perp}$) to the polarization direction of the laser electric field. If

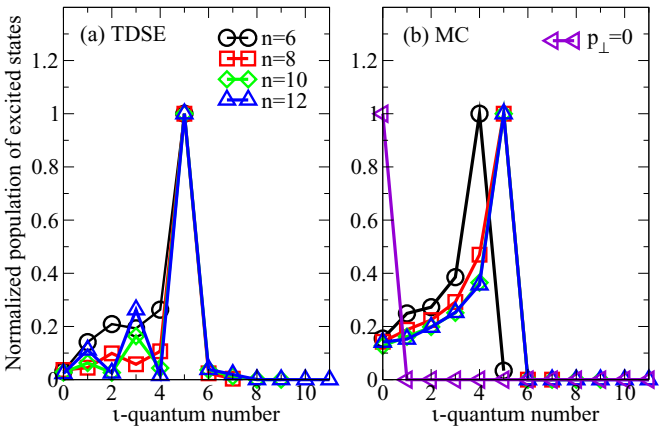

FIG. 3. (Color online) Normalized l distribution of the population of excited states when the n quantum number takes values of $n = 6$ (circles), $n = 8$ (squares), $n = 10$ (diamonds), and $n = 12$ (triangles) (a) from TDSE calculations and (b) full MC simulations. The typical l distribution from MC simulations with $p_\perp = 0$ (sideways triangles) is also presented in (b) for comparison. The laser parameters are the same as in Fig. 2.

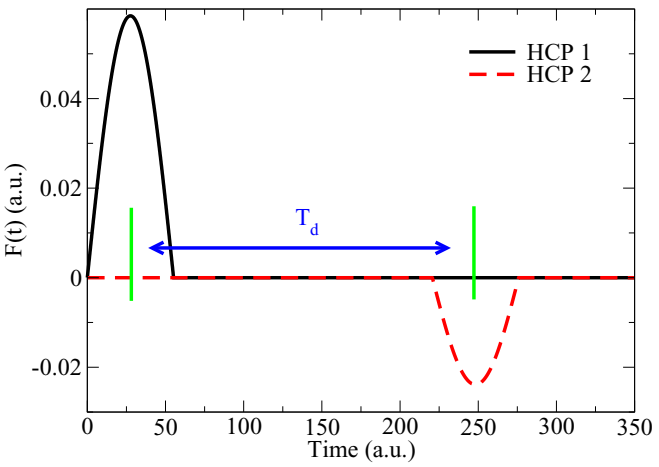

FIG. 4. (Color online) Visualization of two HCP pulses with a time delay T_d between the peak electric fields. The intensities of the two pulses are 1.2×10^{14} and 0.2×10^{14} W/cm^2, respectively. The time delay is $T_d = 2$ T.

the parallel component $V_{c||}$ is set to zero, the change in the population is small compared to the full result. However, if the perpendicular component $V_{c\perp}$ is set to zero, the population is greatly suppressed. This result originates from the Coulomb focusing effect [29,36]. During the propagation, the amplitude of lateral momentum decreases due to Coulomb focusing, which focuses parts of the electron wave function, increasing the efficiency of rescattering. This population suppression shows that the initial lateral momentum is important since the perpendicular force acts only on the lateral momentum. On the other hand, by setting the initial lateral momentum $p_\perp$ to zero, a suppression similar to the case of $V_{c\perp} = 0$ is observed in the population, which demonstrates that in the full MC simulation the dominant contribution comes from electrons with an initial lateral momentum that is close to but not zero. This agrees with the conclusion that the captured electron has a not too large transverse velocity in Ref. [13]. Upon rescattering, the nonzero lateral momentum will result in a nonvanishing angular momentum [see Eq. (11)]. To check this, the l-dependent populations of excited states are compared in Fig. 3. In experiment, the l distributions can be measured with the l-state selective field ionization [37]. The n quantum number takes values of 6, 8, 10, and 12, respectively. The MC simulation with zero $p_\perp$ yields only the $l = 0$ states, and in Fig. 3(b) a single line is presented for $p_\perp = 0$. For comparison, the results are normalized to the maximum. As expected, for the TDSE and full MC simulations, the states with nonzero l numbers exist and even overrun the $l = 0$ part. Note that due to the Coulomb focusing, the distributions in the l quantum number center mostly at the smaller l part.

The above investigations show that both the Coulomb force and initial later momentum are important in the generation of excited states. The initial lateral momentum affects the l distribution of the population, and the Coulomb force plays an important role in the lateral direction. But what about the Coulomb force in the parallel direction? These effects may be stronger for higher-lying Rydberg states, while the n quantum number of the most populated Rydberg states centers at small values (typically less than 10) for multicycle laser pulses. For helium atoms, the n distribution of the population of excited states has a similar sharp peak with a maximum around $n = 8$ at an intensity of 10^{15} W/cm^2 [3]. Also, the dynamics of the electron is complicated for multicycle pulses, making it difficult to investigate the physical mechanism for the formation of Rydberg states. In the following the more simplified tool of HCP fields are utilized.

To generate very high lying Rydberg states, we have utilized a pair of HCPs. The HCP pair is visualized in Fig. 4. A positive-field HCP (HCP 1) is followed by a negative-field HCP (HCP 2), with a time delay T_d between the peak electric fields. HCP 1 serves as a "pump" field, which kicks the electron in the ground state and initiates an outgoing electron wave packet. The "probe" field HCP 2 kicks the outgoing electron in the reverse direction and traps it in the high-lying excited states. With maximum intensities of the two pulses fixed at 1.2×10^{14} and 0.2×10^{14} W/cm^2 with varying time delay, the n distributions of the population of excited states from TDSE calculations are presented in Fig. 5. As T_d increases, the peak in the distribution moves to higher n quantum states. For $T_d = 0.5$ T, the head and rear of these two HCPs meet, and a complete optical cycle is formed. The peak is found at $n = 6$, in agreement with the long-pulse case (see Fig. 2). The position of the peak shifts to $n = 15$ at $T_d = 3.5$ T. To verify this kicking-trapping scenario, we also perform simulations employing only the first HCP. The peaks in the distribution disappear in this single-HCP case, showing that the electron is really trapped by HCP 2. If we use both HCPs but project out all the bound states ($E < 0$) after the interaction of HCP 1, the distribution is nearly the same as for the full simulation. The continuum wave function initiated by HCP 1 is responsible for the generation of excited states.

The n quantum number of the most populated Rydberg states and the corresponding populations using these HCPs from MC simulations are compared in Fig. 6. The TDSE results, which are extracted from Fig. 5, are also given for

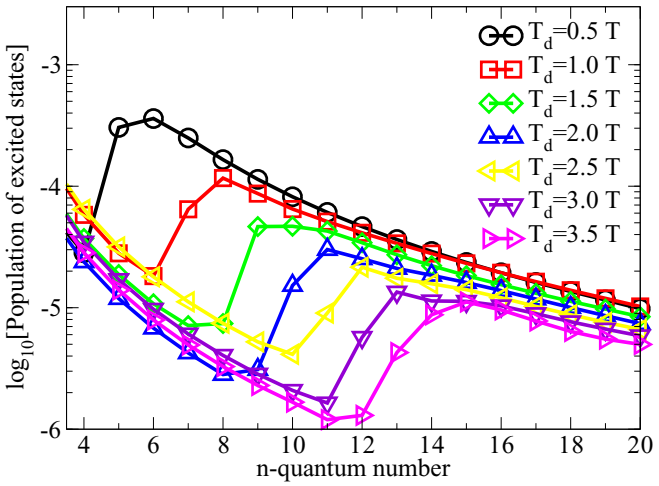

FIG. 5. (Color online) n distribution of the population of excited states from TDSE calculations with two time-delayed HCPs. The intensities of the two pulses are 1.2×10^{14} and 0.2×10^{14} W/cm^2, respectively. The time delay T_d is in units of optical cycles, varying from 0.5 to 3.5.

comparison. Both the n quantum number and the population from full MC simulations are in good agreement with TDSE results. The shift in the maximum position can be explained by the energy change due to the interaction of the ionized electron with the second HCP. The energy change upon HCP 2 reads [17]

$$\Delta E = \mathbf{p}_t \cdot \Delta\mathbf{p} + \Delta p^2/2, \tag{12}$$

where the momentum kick $\Delta\mathbf{p} = -\int \mathbf{F}(t)dt$. For a fixed kick momentum $\Delta\mathbf{p}$, ΔE depends on the electron momentum $\mathbf{p}_t$ at the instant of kicking time t, which, however, depends on the distance r_t between the outgoing electron and the nucleus. During the field-free propagation between the two HCP fields (see Fig. 4), due to the energy conservation $E_0 = p_t^2/2 - 1/r_t$, the farther the distance r_t is, the smaller the momentum $|\mathbf{p}_t|$ will be, leading to the shift in the most populated Rydberg states. The Coulomb force is weak in the asymptotic region ($r \gg 0$), which is ignored in the classical propagation of the three-step model [4]. However, our results show that the generation of highly excited Rydberg states is sensitive to the Coulomb field, even in the asymptotic region, due to the small energy difference between adjacent Rydberg states ($\Delta E_n \propto 1/n^3 \ll 0$ for $n \gg 1$). In Fig. 6(b), the population at the peak distribution decreases with increasing time delay T_d. This decrease originates from the lateral wave-packet dispersion. We turn to the MC simulations with $p_\perp = 0$. In Fig. 6(a), the MC simulations with $p_\perp = 0$ yield results that qualitatively agree with TDSE and full MC calculations. The agreement is due to full incorporation of the Coulomb force in the parallel direction. In Fig. 6(b), for the MC simulation with $p_\perp = 0$, although the maximum population still displays a slight decay, the decaying rate is much smaller than the TDSE and full MC cases, where lateral dispersion is considered.

The lateral momentum plays an important role not only in the absolute population of the most populated Rydberg states but also in the normalized n distribution of the population. For example, in Fig. 7 we present the n distribution of the population of excited states at a time delay of $T_d = 3.0$ T. The TDSE result is extracted from Fig. 5. The MC simulation with $p_\perp$ predicts a narrow distribution, similar to the multi-cycle pulse (MCP) case except for a shift in the position of the peak (Fig. 2). However, the TDSE and full MC calculations predict much broader distributions, especially for the highly excited states. This is different from the MCP case where the TDSE and full MC calculations yield narrow distributions as well. The agreement between TDSE and full MC results demonstrates the accuracy of the initial lateral momentum distribution given by the ADK tunneling theory [Eq. (8)]. The

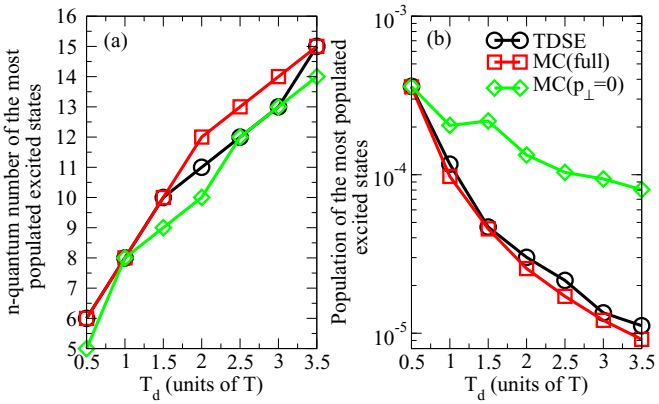

FIG. 6. (Color online) (a) The n quantum number of the most populated Rydberg states and (b) the corresponding populations vs the time delay T_d between two HCPs from TDSE calculations (circles) and MC simulations with (squares) and without (diamonds) the lateral momentum distribution. The populations from MC simulations have been normalized to the TDSE calculation at $T_d = 0.5$ T in (b). The laser parameters are the same as in Fig. 5.

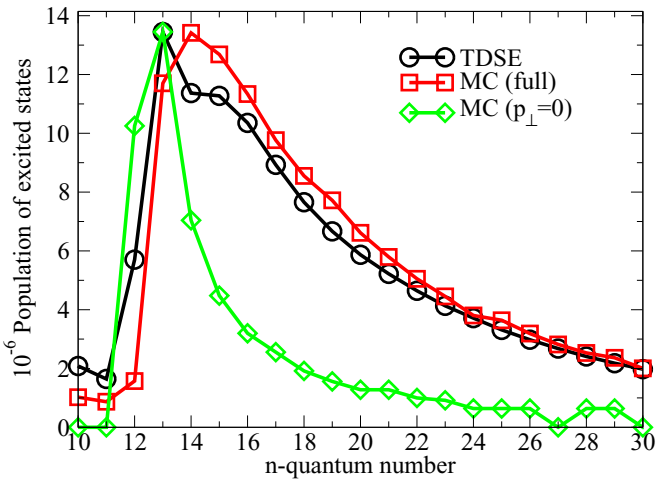

FIG. 7. (Color online) n distribution of the population of excited states from a TDSE calculation (circles) and MC simulations with (squares) and without (diamonds) the initial transverse-momentum distribution. The populations from the MC simulations have been normalized to the maximum of the TDSE calculation at $n = 13$. The intensities of the two pulses are 1.2×10^{14} and 0.2×10^{14} W/cm^2, respectively, with a time delay of $T_d = 3.0$ T.

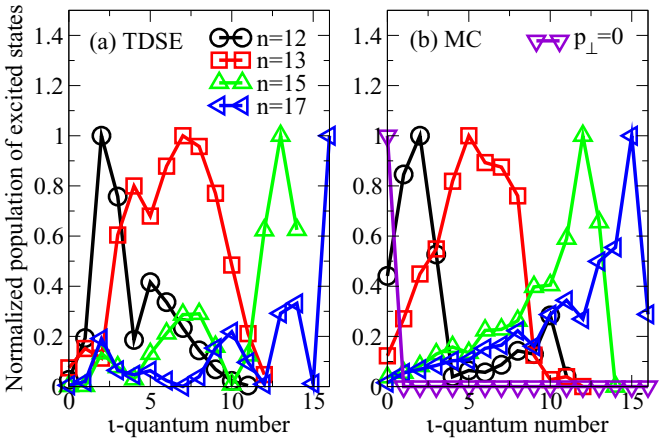

FIG. 8. (Color online) Normalized l distribution of the population of excited states when the n quantum number takes values of $n = 12$ (circles), $n = 13$ (squares), $n = 15$ (triangles), and $n = 17$ (side-ways triangles) from (a) TDSE calculations and (b) full MC simulations. The typical l distribution from MC simulations with $p_\perp = 0$ (upsidedown triangles) is also presented in (b) for comparison. The laser parameters are the same as in Fig. 7.

width of the n distribution may be used as a tool to measure the lateral momentum distribution for the tunnel ionization.

To investigate how the lateral momentum broadens the n distribution in detail, we calculate the l distributions for several n quantum numbers, as presented in Fig. 8. A gradual change in the l distributions is observed with increasing n. For $n = 12$, which lies on the rapid rising edge before the peak distribution, the major contribution comes from the low l quantum states ($l_{\max} = 2$). For the peak distribution at $n = 13$, the intermediate l quantum states contribute the most. On the slowly decaying side, the high l states dominate the distribution for $n = 15$ (and for $n > 15$). The full MC simulations predict results that qualitatively agree with TDSE. Setting the initial lateral momentum to zero, only the $l = 0$ state contributes for each n quantum number. This explains the difference of the distribution width in Fig. 7. In contrast to the MCP case where the l distribution is limited to the small l states, the l distribution can reach high l states in the HCP case. In the MCP case, the Coulomb focusing effect is enhanced in the multiple-return case of the tunneled electron with multicycle laser pulses [38]. In the HCP case, however, the tunneled electron does not need to return to the vicinity of the nucleus. Thus Coulomb focusing is weakened, and high-angular-momentum states can be formed. The Rydberg states with high l values ($l \sim n$) can have very long lifetimes ($\tau_l \propto n^3 l^2$) [25]. With properly chosen parameters, this HCP pair scheme may provide a universal way to selectively excite atoms into an arbitrary nl state. The time delay between the two HCP fields controls the energy, so it also controls the principal n quantum number of the Rydberg states. The lateral momentum is related to the impact parameter b; thus angular momentum $\mathbf{L} = \mathbf{b}\times\mathbf{v}$ and the l quantum number can be determined.

V. CONCLUSIONS AND OUTLOOK

In conclusion, we have investigated the generation of Rydberg states of hydrogen atoms with intense laser pulses. The theoretical methods we use include the TDSE and classical-trajectory MC simulation. For the multicycle pulses, the sum population of highly excited Rydberg states increases rapidly at lower laser intensities and reaches a plateau at higher intensities due to the stabilization of Rydberg atoms in superintense laser fields. The n quantum number of the maximum population of excited states is insensitive to the laser intensity. A sharp maximum in the n distribution of excited states from TDSE calculations is reproduced by the full MC simulations. The initial lateral momentum is responsible for the nonzero l quantum states, and the Coulomb force plays an important role in the lateral direction due to the Coulomb focusing effect.

For the half-cycle pulses, as the time delay between the two HCPs increases, the peak in the distribution shifts to higher n quantum states. This originates from the energy conservation due to the Coulomb force in the asymptotic region, where the energy difference between adjacent Rydberg states is comparable to the Coulomb force. The lateral wave-packet dispersion results in the decreasing of the population at the peak distribution. The major contribution comes from the low l quantum states for low n quantum states, while the high l quantum part dominates the highly excited states. High l states are generated because of the weakening of Coulomb focusing in the asymptotic region.

Our single-electron results also have implications for the generation of Rydberg states in multielectron atoms [39]. In this paper, the discussions are limited to the tunnel ionization regime. With more intense laser fields, the over-the-barrier regime will be reached and different characteristics compared to the tunnel ionization case may be expected. The study of the over-the-barrier regime, which requires a microcanonical distribution [40] instead of the one given by Eqs. (7) and (8), is in progress.

ACKNOWLEDGMENTS

This work is supported by the National Basic Research Program of China (973 Program) under Grant No. 2013CB922203, the NSF of China (Grant No. 11374366), and the Major Research plan of NSF of China (Grant No. 91121017). B.Z. is supported by the Innovation Foundation of NUDT under Grant No. B110204 and the Hunan Provincial Innovation Foundation for Postgraduate under Grant No. CX2011B010.

[1] M. V. Ammosov, N. B. Delone, and V. P. Krainov, Zh. Eksp. Teor. Fiz. **91**, 2008 (1986) [Sov. Phys. JETP **64**, 1191 (1986)].
[2] F. Krausz and M. Ivanov, Rev. Mod. Phys. **81**, 163 (2009).
[3] T. Nubbemeyer, K. Gorling, A. Saenz, U. Eichmann, and W. Sandner, Phys. Rev. Lett. **101**, 233001 (2008).
[4] P. B. Corkum, Phys. Rev. Lett. **71**, 1994 (1993).

[5] M. Lewenstein, Ph. Balcou, M. Yu. Ivanov, A. L'Huillier, and P. B. Corkum, Phys. Rev. A **49**, 2117 (1994).
[6] A. S. Landsman, A. N. Pfeiffer, C. Hofmann, M. Smolarski, C. Cirelli, and U. Keller, New J. Phys. **15**, 013001 (2013).
[7] H. Liu, Y. Q. Liu, L. B. Fu, G. G. Xin, D. F. Ye, J. Liu, X. T. He, Y. D. Yang, X. R. Liu, Y. K. Deng, C. Y. Wu, and Q. H. Gong, Phys. Rev. Lett. **109**, 093001 (2012).
[8] J. Wu, M. Meckel, S. Voss, H. Sann, M. Kunitski, L. Ph. H. Schmidt, A. Czasch, H. Kim, T. Jahnke, and R. Dörner, Phys. Rev. Lett. **108**, 043002 (2012).
[9] B. Zhang, J. M. Yuan, and Z. X. Zhao, Phys. Rev. Lett. **111**, 163001 (2013).
[10] C. P. Liu and K. Z. Hatsagortsyan, Phys. Rev. Lett. **105**, 113003 (2010).
[11] S. P. Goreslavski, G. G. Paulus, S. V. Popruzhenko, and N. I. Shvetsov-Shilovski, Phys. Rev. Lett. **93**, 233002 (2004).
[12] H. G. Muller, Phys. Rev. Lett. **83**, 3158 (1999).
[13] N. I. Shvetsov-Shilovskia, S. P. Goreslavskia, S. V. Popruzhenkoa, and W. Beckerb, Laser Phys. **19**, 1550 (2009).
[14] N. B. Delone and V. P. Krainov, J. Opt. Soc. Am. B **8**, 1207 (1991).
[15] J. Preclíková, M. Kozák, D. Fregenal, Ø. Frette, B. Hamre, B. T. Hjertaker, J. P. Hansen, and L. Kocbach, Phys. Rev. A **86**, 063418 (2012).
[16] R. B. Vrijen, G. M. Lankhuijzen, and L. D. Noordam, Phys. Rev. Lett. **79**, 617 (1997).
[17] A. Wetzels, A. Gürtler, L. D. Noordam, F. Robicheaux, C. Dinu, H. G. Muller, M. J. J. Vrakking, and W. J. van der Zande, Phys. Rev. Lett. **89**, 273003 (2002).
[18] C. Wesdorp, F. Robicheaux, and L. D. Noordam, Phys. Rev. Lett. **87**, 083001 (2001).
[19] A. Wetzelsa, A. Gürtler, H. G. Muller, and L. D. Noordam, Eur. Phys. J. D **14**, 157 (2001).
[20] T. J. Bensky, G. Haeffler, and R. R. Jones, Phys. Rev. Lett. **79**, 2018 (1997).
[21] R. R. Jones, Phys. Rev. Lett. **76**, 3927 (1996).
[22] C. Raman, C. W. S. Conover, C. I. Sukenik, and P. H. Bucksbaum, Phys. Rev. Lett. **76**, 2436 (1996).
[23] L. D. Noordam, H. Stapelfeldt, D. I. Duncan, and T. F. Gallagher, Phys. Rev. Lett. **68**, 1496 (1992).
[24] S. X. Hu and L. A. Collins, Phys. Rev. A **69**, 041402(R) (2004).
[25] T. F. Gallagher, Rep. Prog. Phys. **51**, 143 (1988).
[26] W. H. Press, S. A. Teukolsky, W. T. Vetterling, and B. P. Flannery, *Numerical Recipes*, 3rd ed. (Cambridge University Press, New York, 2007).
[27] X. M. Tong and S.-I. Chu, Chem. Phys. **217**, 119 (1997).
[28] B. Zhang, J. M. Yuan, and Z. X. Zhao, Phys. Rev. A **85**, 033421 (2012).
[29] T. Brabec, M. Y. Ivanov, and P. B. Corkum, Phys. Rev. A **54**, R2551 (1996).
[30] G. L. Yudin and M. Y. Ivanov, Phys. Rev. A **63**, 033404 (2001).
[31] J. S. Cohen, Phys. Rev. A **64**, 043412 (2001).
[32] L. V. Keldysh, Zh. Eksp. Teor. Fiz. **47**, 1945 (1965) [Sov. Phys. JETP **20**, 1307 (1965)].
[33] C. L. Lawson, R. J. Hanson, D. Kincaid, and F. T. Krogh, ACM Trans. Math. Software **5**, 308 (1979); **14**, 1 (1988); **16**, 1 (1990).
[34] E. Anderson, Z. Bai, C. Bischof, S. Blackford, J. Demmel, J. Dongarra, J. Du Croz, A. Greenbaum, S. Hammarling, A. McKenney, and D. Sorensen, *LAPACK Users Guide*, 3rd ed. (Society for Industrial and Applied Mathematics, Philadelphia, 1999).
[35] U. Eichmann, A. Saenz, S. Eilzer, T. Nubbemeyer, and W. Sandner, Phys. Rev. Lett. **110**, 203002 (2013).
[36] D. Comtois, D. Zeidler, H. Pépin, J. C. Kieffer, D. M. Villeneuve, and P. B. Corkum, J. Phys. B **38**, 1923 (2005).
[37] A. Gürtler and W. J. van der Zande, Phys. Lett. A **324**, 315 (2004).
[38] V. R. Bhardwaj, S. A. Aseyev, M. Mehendale, G. L. Yudin, D. M. Villeneuve, D. M. Rayner, M. Yu. Ivanov, and P. B. Corkum, Phys. Rev. Lett. **86**, 3522 (2001).
[39] K. N. Shomsky, Z. S. Smith, and S. L. Haan, Phys. Rev. A **79**, 061402 (2009).
[40] P. Botheron and B. Pons, Phys. Rev. A **80**, 023402 (2009).